Direct extraction of phase dynamics from fluctuating rhythmic data based on a Bayesian approach

Kaiichiro Ota* and Toshio Aoyagi†
Graduate School of Informatics, Kyoto University, Kyoto 606-8501, Japan and
JST CREST, Sanbancho, Chiyoda-ku, Tokyo 102-0075, Japan
(Dated: May 19, 2014)

Employing both Bayesian statistics and the theory of nonlinear dynamics, we present a practically efficient method to extract a phase description of weakly coupled limit-cycle oscillators directly from time series observed in a rhythmic system. As a practical application, we numerically demonstrate that this method can retrieve all the interaction functions from the fluctuating rhythmic neuronal activity exhibited by a network of asymmetrically coupled neurons. This method can be regarded as a type of statistical phase reduction method that requires no detailed modeling, and as such, it is a very practical and reliable method in application to data-driven studies of rhythmic systems.

arXiv:1405.4126v1 [nlin.AO] 16 May 2014

* kaiichiro@acs.i.kyoto-u.ac.jp
† aoyagi@i.kyoto-u.ac.jp

Theoretical models have provided great insight into the nature of real-world dynamic phenomena [1–4]. In general, to understand some phenomena of interest, we need to construct a good theoretical model that accounts for experimental data. Successful theoretical models can be roughly divided into two classes. One class consists of detailed models constructed to faithfully reproduce as many characteristics of the systems under study as possible. Such models contribute to the quantitative understanding of the dynamical behavior of the specific systems to which they are applied. The other class consists of abstract models constructed to capture some essential aspect of the systems of interest, such as rhythmic behavior. This type of model is not intended to accurately simulate all the dynamical behavior of a specific system, but rather to provide a description of some universal aspect of its dynamics. The advantage of this type of model is that, because it does not focus on the detailed behavior of any specific system, but rather on the universal aspects of this behavior, it can provide a unified framework for describing the behavior exhibited by a wide range of dynamical systems. In this way, such models allow us to gain a deeper understanding of the universal mechanisms existing in broad classes of systems.

One successful model of the abstract type described above is the phase description of the dynamics of interacting oscillatory systems (Fig. 1). In such a model, the evolution of each oscillatory system is described by a single degree of freedom, the phase. In this description, the dynamics of a system of N coupled oscillators is generally described by a set of equations of the form

$$\frac{d\phi_i}{dt} = \omega_i + \sum_{j\neq i}^{N} \Gamma_{ij}(\phi_j - \phi_i) \quad (i = 1, \ldots, N), \tag{1}$$

where ϕ_i is the phase of the i-th oscillator, representing the timing of its oscillation [5]. The parameter ω_i and the function $\Gamma_{ij}(\Delta\phi)$ denote the natural frequency of the i-th oscillator and the coupling function from the j-th oscillator to i-th oscillator, respectively. These coupling functions and natural frequencies can be theoretically determined using a detailed model of the form $\frac{d\boldsymbol{X}_i}{dt} = \boldsymbol{F}_i(\boldsymbol{X}_i) + \sum_{j\neq i}^{N} \boldsymbol{G}_{ij}(\boldsymbol{X}_i, \boldsymbol{X}_j)$ (where $\boldsymbol{X}_i$ denotes the multidimensional state of the i-th oscillator), whose dynamics generally have a large number of degrees of freedom. In fact, it has been found that, employed in this manner, the theory of dynamical systems allows for the construction of models of the form (1) that provide descriptions of a broad class of systems of limit-cycle oscillators. Specifically, this class consists of those systems in which the interactions between oscillators only affect the phase asymptotically. In particular, it has been found that rhythmic systems of diverse types can be treated by models of this form [6].

The conventional method for constructing the phase oscillator model for a specific system consists of two steps: In the first, a detailed model is constructed from experimental data, and in the second, a phase model of the form (1) is derived from this detailed model by applying the phase reduction theory (Fig. 1). However, it is often unfeasible to construct the correct detailed model in one step, because the underlying dynamics are generally nonlinear and of high dimension. For this reason, derivation of the phase model using the conventional approach is often quite complicated and time consuming. In this Letter, we propose an alternative approach to describing the dynamics of such a network that forgoes the detailed model used in the conventional approach and, instead, begins with (1), slightly generalized to include a noise term as

$$\frac{d\phi_i}{dt} = \omega_i + \sum_{j\neq i}^{N} \Gamma_{ij}(\phi_j - \phi_i) + \eta_i(t). \tag{2}$$

In our approach, we skip the first step of the conventional approach and determine the explicit content of the phase model given in (2) directly from time-series data (Fig. 1). This can be regarded as a statistical version of the phase

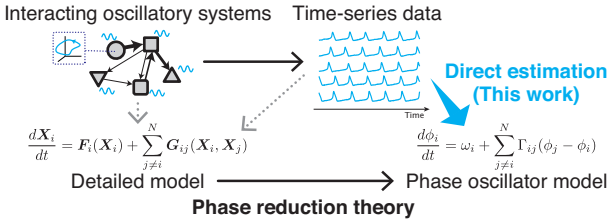

FIG. 1. Conceptual diagram of the method for obtaining phase dynamics from observed rhythmic time series. In the conventional approach, we first construct a detailed model based on experimental observations and next obtain the phase oscillator model by applying the phase reduction method to this detailed model. Our proposed alternative approach begins with a phase oscillator model of generic form. We then determine through use of a Bayesian statistical method the explicit content of this model directly from the observed time-series data, without constructing the detailed model. This can be regarded as a statistical phase reduction method based on Bayesian theory.

reduction method based on Bayesian theory. Here, we introduce the noise $\eta_i(t)$, which represents an unavoidable source of uncertainty, for example, arising from observational error. For simplicity, we assume that each noise function $\eta_i(t)$ is independent Gaussian white noise satisfying $\langle \eta_i(t) \rangle = 0, \langle \eta_i(t)\eta_j(s) \rangle = 2D_i\delta_{ij}\delta(t-s)$, where δ_{ij} is the Kronecker delta and D_i represents the strength of the noise. Thus, in the approach we propose, we must determine the nonlinear coupling functions $\Gamma_{ij}(\Delta\phi)$ and the model parameters ω_i and D_i in the dynamical system (2) so as to best predict the dynamical behavior of the observed system. This is a typical nonlinear optimization problem. Such problems are often difficult to treat because there generally exist many local optimal solutions, owing to the nonlinearity. To overcome this difficulty, we employ a Bayesian statistical approach, which allows us to derive the phase oscillator model directly from the time-series data [7–14].

Consider the situation in which we observe N oscillatory signals, $s_i(t)\,(i = 1, \ldots, N)$, each of which is generated by a separate limit-cycle oscillator, and suppose that these oscillators are weakly coupled. Further, we assume that each signal $s_i(t)$ is sampled at $T+1$ discrete time points $t_\tau = t_1 + (\tau - 1)\Delta t$, where $\tau = 1, 2, \ldots, T+1$ and Δt is the sampling interval.

Our method consists of two main steps In the first step, we transform each observed signal into a time series of the phase (Fig. 2b). For this purpose, using the Hilbert transformation $s_i^{\mathcal{H}}(t)$ of the signal $s_i(t)$, we construct a prototype of the phase $\theta_i(t)$, as defined by $A_i(t)e^{i\theta_i(t)} = s_i(t) + is_i^{\mathcal{H}}(t)$ [15]. However, the variable θ_i here generally differs from the phase ϕ_i used in the phase description (2), because θ_i does not increase with time at a constant rate in the absence of both interactions and noise. In the context of dynamical systems described by (2), the phase should be chosen as a quantity that changes in time at a constant rate in the absence of noise and interactions. Using the fact that the probability density distribution of θ_i, $f(\theta_i)$, is inversely proportional to $d\theta_i/dt$ statistically, Kralemann *et al.* proposed the following transformation from the prototype phase θ_i to the phase ϕ_i: $\phi(\theta) = 2\pi \int_0^\theta f(\theta')d\theta'$ [10–12]. With the above two procedures, we can transform the observed signals $s_i(t_\tau)$ into N time series of the phase $\phi_i(t_\tau)$ $(\tau = 1, 2, \cdots, T+1)$, which are expected to increase linearly with time in the absence of noise and interactions. In general, the presence of noise and interactions causes slight fluctuations of the phases. These fluctuations contain information from which the explicit content of (2) can be inferred.

As an illustrative example, we applied the method described above to a system of two coupled van der Pol oscillators,

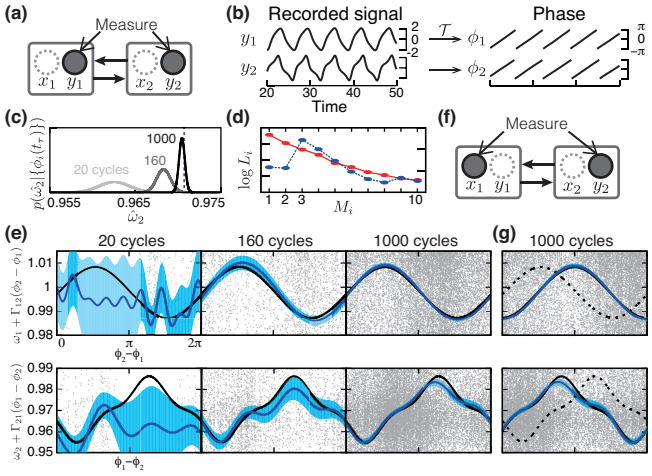

FIG. 2. Phase description extracted directly from rhythmic signals in a system of two mutually coupled van der Pol oscillators [16]. From the two state variables of each oscillator, only the variable $y_i(t)$ is observed as a signal, as depicted in (a). (b) The recorded signals $y_i(t)$ (left graphs) are transformed into phase time series $\phi_i(t)$ (right graphs). Both $y_i(t)$ and $\phi_i(t)$ fluctuate slightly, owing to the interactions and noise, though the fluctuations are difficult to discern here. Typical data taken over approximately five oscillation cycles are plotted. (c) Posterior probability density distribution of $\hat{\omega}_2$ calculated for three observation durations. The dashed vertical line represents the theoretical value. (d) Log marginal likelihood for various values of M_i in the case of the data measured with 1000 oscillation cycles. Following the Bayesian model selection, we choose the value M_i giving the largest marginal likelihood. The log marginal likelihoods for $\hat{\Gamma}_{12}$ (red solid curve) and $\hat{\Gamma}_{21}$ (blue dashed curve) have maximum values at $M_1^* = 1$ and $M_2^* = 3$, respectively. (e) Posterior distributions for the deterministic terms $\omega_i + \Gamma_{ij}(\Delta\phi)$. The blue curves and the light blue regions represent the mean and 95% confidence interval of the distribution, respectively. The black curves are those obtained from the phase reduction theory, and the numerous gray dots denote data points. The graphs in each column display the results obtained using the data measured with the three different time durations. (f,g) Here, it is seen that even if different types of dynamical variables (i.e., x_1 and y_2) are used as the signals (panel f), the phase coupling functions can still be reliably retrieved, except for an inevitable uncertainty in the phase shift (see panel g and the main text). For comparison, the dashed curves represent the theoretical curves with the correct phase relationship.

as shown in Fig. 2. For the parameter values used there, each oscillator exhibits limit-cycle oscillation in the absence of coupling. Here we assume that for the i-th oscillator only the time-series of the variable y_i can be observed as the signal, $s_i(t)$ (i.e., x_i is unobservable), as illustrated in Fig. 2a. Figure 2b exhibits a typical result of the transformation from the signals y_i to the phases ϕ_i.

The second step is to determine the explicit content of the phase oscillator model (2) needed to generate the obtained phase time-series $\phi_i(t_\tau)$. First, we specify all of the parameters to be evaluated. The 2π-periodic coupling function Γ_{ij} can be expanded in a Fourier series as $\Gamma_{ij}(\Delta\phi) = a_{ij}^{(0)} + \sum_{m=1}^{M_i}\left[a_{ij}^{(m)}\cos(m\Delta\phi) + b_{ij}^{(m)}\sin(m\Delta\phi)\right]$. In this expansion, we keep only up to the M_i-th harmonic for each Γ_{ij}. The parameters M_i control the complexity of the model and can be determined using a model selection method, as explained below. Except in certain particular situations, $\{a_{ij}^{(0)}\}_{j\neq i}$ and ω_i are redundant, because their contributions to the dynamics are inseparable [11]. We therefore treat $\hat{\omega}_i \equiv \omega_i + \sum_{j\neq i}^{N} a_{ij}^{(0)}$ as a single parameter. Thus, in all, we must evaluate $2+2M_i(N-1)$ unknown model parameters, $\hat{\omega}_i$, D_i and $\{a_{ij}^{(m)}, b_{ij}^{(m)}\}_{m,j}$. For simplicity, hereafter we use the shorthand notation $\boldsymbol{c}_i \equiv [\hat{\omega}_i, \boldsymbol{c}_{i,1}, \cdots, \boldsymbol{c}_{i,i-1}, \boldsymbol{c}_{i,i+1}, \cdots, \boldsymbol{c}_{i,N}]^{\mathrm{T}}$, with $\boldsymbol{c}_{i,j} \equiv \left[a_{ij}^{(1)}, b_{ij}^{(1)}, a_{ij}^{(2)}, b_{ij}^{(2)}, \cdots, a_{ij}^{(M_i)}, b_{ij}^{(M_i)}\right]$ and $\psi_{ij} \equiv \phi_j - \phi_i$.

We next evaluate the above parameters from the phase time-series $\{\phi_i(t_\tau)\}$ $(i = 1, \ldots, N; \tau = 1, \ldots, T+1)$ on the basis of the Bayesian statistical framework [17, 18]. First, we write the probability to reproduce the observed phase time series $\{\phi_i(t_\tau)\}$ given $\boldsymbol{c}_i$ and D_i as

$$p(\{\phi_i(t_\tau)\}|\boldsymbol{c}_i, D_i) = \prod_{\tau=1}^{T} \mathcal{N}\left(\hat{\omega}_i + \sum_{j\neq i}^{N} \hat{\Gamma}_{ij}[\psi_{ij}(t_\tau)], \sigma_i^2\right), \tag{3}$$

where $\hat{\Gamma}_{ij}(\Delta\phi) \equiv \Gamma_{ij}(\Delta\phi) - a_{ij}^{(0)}$ and $\sigma_i^2 \equiv \frac{2D_i}{\Delta t}$. Here, $\mathcal{N}(\mu, \sigma^2)$ denotes the density of the Gaussian distribution with mean μ and variance σ^2. Next, following the standard Bayesian approach, we introduce a probability density distribution of the unknown parameters written $p(\boldsymbol{c}_i, D_i)$, which allows us to compute not only the most probable parameter values (maximum likelihood estimates) but also their uncertainties. When we obtain new observed data $\{\phi_i(t_\tau)\}$, the parameter distribution $p(\boldsymbol{c}_i, D_i)$ is updated according to Bayes' theorem,

$$p(\boldsymbol{c}_i, D_i|\{\phi_i(t_j)\}) \propto p(\{\phi_i(t_j)\}|\boldsymbol{c}_i, D_i)p(\boldsymbol{c}_i, D_i), \tag{4}$$

where $p(\boldsymbol{c}_i, D_i)$ and $p(\boldsymbol{c}_i, D_i|\{\phi_i(t_j)\})$ are called the "prior" and "posterior" distributions, respectively. Although the choice of the functional form of the prior distribution is somewhat arbitrary, it is convenient to use a conjugate prior distribution so that the posterior distribution derived from (4) has the same functional form as the prior distribution. In particular, if the conjugate prior distribution can be characterized by some parameters (called hyperparameters), we have only to update the values of the hyperparameters to obtain the posterior distribution. For the conjugate prior distribution, we adopt a Gaussian-inverse-gamma distribution [16], given by

$$p(\boldsymbol{c}_i, D_i) \propto e^{-\frac{(\boldsymbol{c}_i - \boldsymbol{\chi}_i)^{\mathrm{T}}\Sigma_i^{-1}(\boldsymbol{c}_i - \boldsymbol{\chi}_i) + 2\beta_i}{2\sigma_i^2}} (\sigma_i^2)^{-\frac{P_i}{2} - \alpha_i - 1}, \tag{5}$$

where P_i is the dimension of the vector $\boldsymbol{c}_i$. Note that the prior distribution for $\boldsymbol{c}_i$ and D_i is characterized fully by the hyperparameters $\boldsymbol{\chi}_i, \Sigma_i, \alpha_i$ and β_i. Using Eq. (4) with Eqs. (3) and (5), we can easily compute the hyperparameters of the posterior distribution as follows:

$$\begin{aligned}
\boldsymbol{\chi}_i^{\mathrm{new}} &= \Sigma_i^{\mathrm{new}}(F_i^{\mathrm{T}}\boldsymbol{\delta}_i + (\Sigma_i^{\mathrm{old}})^{-1}\boldsymbol{\chi}_i^{\mathrm{old}}),\\
\Sigma_i^{\mathrm{new}} &= \left\{(\Sigma_i^{\mathrm{old}})^{-1} + F_i^{\mathrm{T}}F_i\right\}^{-1},\\
\alpha_i^{\mathrm{new}} &= \alpha_i^{\mathrm{old}} + \frac{T}{2},\\
\beta_i^{\mathrm{new}} &= \beta_i^{\mathrm{old}} + \frac{1}{2}\{\boldsymbol{\delta}_i^{\mathrm{T}}\boldsymbol{\delta}_i + (\boldsymbol{\chi}_i^{\mathrm{old}})^{\mathrm{T}}(\Sigma_i^{\mathrm{old}})^{-1}\boldsymbol{\chi}_i^{\mathrm{old}}\\
&\qquad -(\boldsymbol{\chi}_i^{\mathrm{new}})^{\mathrm{T}}(\Sigma_i^{\mathrm{new}})^{-1}\boldsymbol{\chi}_i^{\mathrm{new}}\}.
\end{aligned}$$

Here we have defined the T-dimensional column vectors $(\boldsymbol{\delta}_i)_\tau \equiv \frac{\phi_i(t_{\tau+1}) - \phi_i(t_\tau)}{\Delta t}$ $(\tau = 1, \ldots, T)$ and the $T \times P_i$ matrices

$$F_i = \begin{bmatrix} 1 & \boldsymbol{G}_{i,1}^1 & \cdots & \boldsymbol{G}_{i,i-1}^1 & \boldsymbol{G}_{i,i+1}^1 & \cdots & \boldsymbol{G}_{i,N}^1 \\ & & & \vdots & & & \\ 1 & \boldsymbol{G}_{i,1}^T & \cdots & \boldsymbol{G}_{i,i-1}^T & \boldsymbol{G}_{i,i+1}^T & \cdots & \boldsymbol{G}_{i,N}^T \end{bmatrix},$$

with the M_i-dimensional row vectors $\boldsymbol{G}^{\tau}_{i,j} \equiv [\cos\psi_{ij}(t_\tau), \sin\psi_{ij}(t_\tau), \cos(2\psi_{ij}(t_\tau)), \sin(2\psi_{ij}(t_\tau)), \cdots, \cos(M_i\psi_{ij}(t_\tau)), \sin(M_i\psi_{ij}(t_\tau))]$. The superscripts "new" and "old" indicate the hyperparameters of the posterior and prior distributions, respectively.

In the case of van der Pol oscillators, a typical form of the posterior distribution for $\hat{\omega}_2$ is displayed in Fig. 2c. The different curves correspond to posterior distributions obtained using observations with different durations. It is seen that as the amount of data is increased, the peak of the posterior distribution becomes sharper and closer to the theoretical value (dashed vertical line). This implies that the estimated mean value becomes both more accurate and more precise as the amount of data increases.

Now we return to the determination of M_i, which controls the degree of approximation of $\hat{\Gamma}_{ij}(\Delta\phi)$ resulting from the truncation of the Fourier series. Bayesian theory provides an effective method to choose the "best" model with certain values of the parameters M_i^*. In this method, using the posterior distributions calculated with Eq. (3) for various values of $M_i = 1, 2, \cdots$, we evaluate the values of the marginal likelihood functions $L_i(M_i) \equiv \int\cdots\int p(\boldsymbol{\phi}_i|\boldsymbol{c}_i, D_i, M_i)d\boldsymbol{c}_i\, dD_i$. It is well known that the quantities L_i measure the goodness of a fit over all possible values of the parameters, taking account of the model's complexity, which is essentially given by the total number of model parameters to be evaluated [17, 18]. Then, it is reasonable to choose the optimal value M_i^* for each M_i such that $L_i(M_i^*) = \max_{M_i}\{L_i(M_i)\}$ [16].

The dependence of the marginal likelihood function on M_i for the case of van der Pol oscillators is plotted in Fig. 2d. Note that L_i generally tends to decrease as a function of M_i for sufficiently large M_i, because the number of free parameters is too large (i.e., the model is too complex). The graph shows that L_1 and L_2 are maximal at $M_1 = 1$ and $M_2 = 3$, respectively. This result implies that the function $\hat{\Gamma}_{12}(\Delta\phi)$ is accurately approximated by only the first Fourier mode, whereas we need to consider up to the third mode for $\hat{\Gamma}_{21}(\Delta\phi)$. Using the posterior distribution obtained with $M_1 = 1$ and $M_2 = 3$, we can calculate the posterior density distribution for the functional form of the deterministic terms $\omega_i + \Gamma_{ij}(\psi_{ij})$, as indicated in Fig. 2e. It is seen that the estimated functions converge to the theoretical ones as the amount of data increases.

It is somewhat surprising that, even if we use a pair of different state variables x_1 and y_2 as the signal sources (Fig. 2f), the result of the estimation is essentially unchanged (Fig. 2g). This suggests that the result is largely insensitive to the choice of the observed signals; in other words, we can use any variables that reflect the rhythmic behavior of each oscillator. This suggests that our method should be widely applicable in various experimental settings. We note that, as shown in Fig. 2g, an uncertainty in the phase shift is inevitable, because even in principle we cannot know the phase relationship between x_1 and y_2 only from the data. However, it is seen that, other than such an inevitable phase shift, the estimation is reasonably accurate.

We next apply our method to a more practical case, in which a network consisting of a larger number of synaptically coupled inhibitory and excitatory neurons is investigated (Fig. 3a), and the neuronal membrane voltages $V_i(t)$ are measured as signals. In addition, we consider more general and realistic experimental conditions, in which only some of the neurons are actively spiking, while others are inactive, as shown in Fig. 3b. In this treatment, we assume that

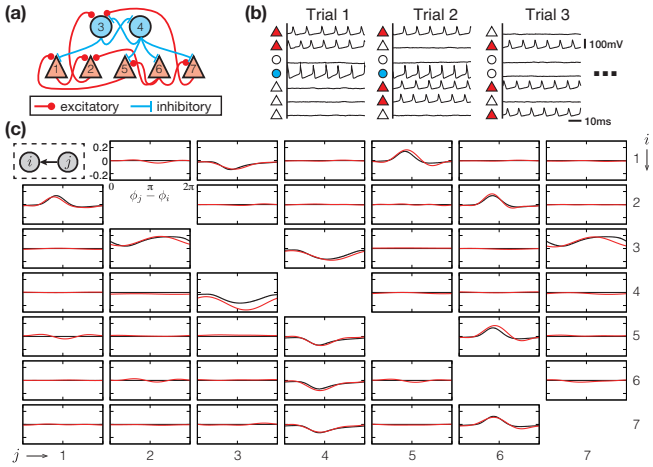

FIG. 3. Extracting phase dynamics from the membrane voltages generated in a network of spiking neurons. (a) Synaptic connections in a network consisting of five excitatory and two inhibitory neurons [16]. (b) Experimental conditions for measuring the neuronal membrane voltages. In each trial, 3 or 4 randomly selected neurons fire, while the others are quiescent. In each case, the selected neurons are injected with different fixed levels of input current, and thus exhibit firing activity at different rates in the range 99–107 Hz. The data set used here consists of 100 trials that contain 3700–4600 spikes for each cell. The time duration of each trial is 1000 ms. (c) Estimated mean curves (red) and theoretical curves (black) for all Γ_{ij}.

the properties of the synaptic connections do not change throughout the measurement procedure. In each trial, we randomly choose only three or four neurons to be activated by injecting the selected neurons with different neuron-specific levels of current. One of the characteristics of the synaptic interaction used here is that inactive neurons are not involved in the interaction and thus have no effect on the dynamics of the system. This means that in a single trial, we can retrieve information only regarding the interactions among the neurons that are active in that trial.

Even with the information limited in the manner described above, by combining the data from sufficiently many experimental trials, we found that with our proposed method, we are able to obtain a phase description directly from the observed time-series data. Figure 3c displays the result for the estimated mean of the coupling functions $\Gamma_{ij}(\Delta\phi)$. We find that the estimated coupling functions are sufficiently close to the theoretical ones that the resulting model correctly discriminates among inhibitory, excitatory and null couplings. It is thus seen that the essential functional aspects of the neuronal network can be reconstructed from the voltage time-series data alone. Furthermore, we have confirmed that the coupling functions can also be successfully evaluated in the case of a larger network [16].

In this Letter, we have proposed an approach for constructing a coupled phase oscillator description of rhythmic behavior directly from fluctuating time-series data. This approach combines the theory of nonlinear dynamics and a Bayesian statistical method. We have demonstrated that this approach allows us to reconstruct the coupling functions in a quantitatively accurate manner, even in the case that only one of the states of each oscillator exhibiting rhythmic behavior is measured. Furthermore, we have confirmed that both the precision and accuracy of the reconstruction are essentially the same in the case that the observed state variables of the oscillators are of different types as in the case that they are of the same type. We thus believe that our method will be quite useful in application to actual experiments and that it will contribute to data-driven studies of various rhythmic phenomena found in biological, physical and social systems.

ACKNOWLEDGMENTS

We thank Y. Iba for useful discussions. This work was supported by KAKENHI 25115719.

SUPPLEMENTAL MATERIAL

I. THE PRIOR DISTRIBUTION AND ITS HYPERPARAMETERS

The full form of a Gaussian-inverse-gamma distribution (Eq. 5 in the main text) is written as

$$p(\boldsymbol{c}, D|\boldsymbol{\chi}, \Sigma, \alpha, \beta) = \frac{1}{(2\pi\sigma^2)^{P/2}|\Sigma|^{1/2}} \exp\left\{-\frac{1}{2\sigma^2}(\boldsymbol{c}-\boldsymbol{\chi})^{\mathrm{T}}\Sigma^{-1}(\boldsymbol{c}-\boldsymbol{\chi})\right\} \frac{\beta^\alpha}{\Gamma(\alpha)}(\sigma^2)^{-\alpha-1}\exp\left(-\frac{\beta}{\sigma^2}\right),$$

where $\sigma^2 \equiv \frac{2D}{\Delta t}$, and we omit the subscripts i to keep the notation uncluttered. This is a conjugate prior distribution for the Gaussian likelihood function given in Eq. 3. By substituting the likelihood (Eq. 3) and prior distribution (Eq. 5) into Bayes' theorem (Eq. 4), it is easily checked that the posterior distribution also has a Gaussian-inverse-gamma form, and thus we obtain the relations for the hyperparameters (Eq. 6).

In the numerical simulations discussed in the main text, the hyperparameters in the prior distributions were initially set as follows. We chose $\boldsymbol{\chi}_i^{\mathrm{old}} = \mathbf{0}$ and $\alpha_i^{\mathrm{old}} = \beta_i^{\mathrm{old}} = 0$, which correspond to the values for an uninformative prior distribution. The covariance matrix Σ_i^{old} was initially chosen to be a diagonal matrix as

$$\Sigma_i^{\mathrm{old}} = \mathrm{diag}[\lambda_i^{-1}, M_i\lambda_i^{-1}, \ldots, M_i\lambda_i^{-1}],$$

and we determined the precision parameters λ_i by maximizing the marginal likelihood, just as we did for M_i (see the next section).

II. APPROXIMATED MAXIMIZATION OF THE MARGINAL LIKELIHOOD

In the analyses presented in the main text, we determined the values of M_i and λ_i by maximizing the log marginal likelihood function L_i, following a Bayesian model selection method. However, because in general we cannot analytically optimize L_i with respect to these parameters, we approximated the optimal parameter values, M_i^* and λ_i^*. Specifically, we considered many points distributed over the plane (M_i, λ_i) as

$$\begin{cases} M_i & = 0, 1, \ldots, M_{\max}, \\ \log\lambda_i & = 0, 1, \ldots, 10, \end{cases}$$

where $M_{\max} = 10$ for the first example and 5 for the second example. For each point (M_i, λ_i), we calculated the posterior distribution and the corresponding value of $L_i(M_i, \lambda_i)$. We then found the point (M_i^*, λ_i^*) that yielded the largest L_i and used it as the optimal value. We note that in Fig. 2d in the main text, we plotted the logarithm of $L_i[M_i, \lambda_i^*(M_i)]$, where $\lambda_i^*(M_i)$ is the optimum under fixed M_i, i.e., $\lambda_i^*(M_i) \equiv \mathrm{argmax}_{\lambda_i} L_i(M_i, \lambda_i)$.

III. MODEL EQUATIONS USED IN THE FIRST EXAMPLE

In the simulations whose results are plotted in Fig. 2 in the main text, we used the van der Pol-type oscillators given by

$$\begin{aligned} \dot{x}_1 &= y_1 + K(x_2 - x_1) + \xi_{x,1}(t), \\ \dot{y}_1 &= \epsilon_1(1-x_1^2)y_1 - x_1 + Kx_2^2y_2 + \xi_{y,1}(t), \\ \dot{x}_2 &= y_2 - Kx_1^2y_1 + \xi_{x,2}(t), \\ \dot{y}_2 &= \epsilon_2(1-x_2^2)y_2 - x_2 + Kx_1y_1^2 + \xi_{y,2}(t), \end{aligned}$$

with $\langle\xi_{a,i}(s)\xi_{b,j}(t)\rangle = \sigma^2\delta_{ij}\delta_{ab}\delta(s-t)$. Parameter values are $\epsilon_1 = 0.3, \epsilon_2 = 0.7, K = 0.01$ and $\sigma = 0.03$.

IV. NEURON AND SYNAPSE MODELS USED IN THE SECOND EXAMPLE

In the simulations whose results are plotted in Fig. 3 in the main text, for each excitatory neuron, we used the Hodgkin-Huxley model [19], given by

$$
\begin{aligned}
C\dot{V} &= G_{\rm Na}m^3h(E_{\rm Na}-V) + G_{\rm K}n^4(E_{\rm K}-V) + G_{\rm L}(E_{\rm L}-V) + I_{\rm input} + \xi_V,\\
\dot{m} &= \alpha_m(V)(1-m) - \beta_m(V)m + \xi_m, \alpha_m(V) = \frac{0.1(V+40)}{1-\exp[(-V-40)/10]}, \beta_m(V) = 4\exp\frac{-V-65}{18},\\
\dot{h} &= \alpha_h(V)(1-h) - \beta_h(V)h + \xi_h, \alpha_h(V) = 0.07\exp\frac{-V-65}{20}, \beta_h(V) = \frac{1}{1+\exp[(-V-35)/10]},\\
\dot{n} &= \alpha_n(V)(1-n) - \beta_n(V)n + \xi_n, \alpha_n(V) = \frac{0.01(V+55)}{1-\exp[(-V-55)/10]}, \beta_n(V) = 0.125\exp\frac{-V-65}{80},
\end{aligned}
$$

with parameter values $C = 1, G_{\rm Na} = 120, G_{\rm K} = 36, G_{\rm L} = 0.3, E_{\rm Na} = 50, E_{\rm K} = -77, E_{\rm L} = -54.4$. For each inhibitory neuron, we used a model of fast-spiking neurons [20], given by

$$
\begin{aligned}
C\dot{V} &= G_{\rm Na}m^3h(E_{\rm Na}-V) + G_{\rm K}n^2(E_{\rm K}-V) + G_{\rm L}(E_{\rm L}-V) + I_{\rm input} + \xi_V,\\
\dot{m} &= \alpha_m(V)(1-m) - \beta_m(V)m + \xi_m, \alpha_m(V) = \frac{40(V-75)}{1-\exp[(75-V)/13.5]}, \beta_m(V) = 1.2262\exp\frac{-V}{42.248},\\
\dot{h} &= \alpha_h(V)(1-h) - \beta_h(V)h + \xi_h, \alpha_h(V) = 0.0035\exp\frac{-V}{24.186}, \beta_h(V) = \frac{0.017(-51.25-V)}{\exp[(-51.25-V)/5.2]-1},\\
\dot{n} &= \alpha_n(V)(1-n) - \beta_n(V)n + \xi_n, \alpha_n(V) = \frac{V-95}{1-\exp[(95-V)/11.8]}, \beta_n(V) = 0.025\exp\frac{-V}{22.222},
\end{aligned}
$$

with parameter values $C = 1, G_{\rm Na} = 112, G_{\rm K} = 224, G_{\rm L} = 0.1, E_{\rm Na} = 55, E_{\rm K} = -97, E_{\rm L} = -70.0$.

For each cell i, the input current was the sum of the bias and synaptic currents: $I_{{\rm input},i} = I_{{\rm bias},i} + \sum_{j\in{\rm pre}_i} I_{{\rm syn},ij}$. Here, ${\rm pre}_i$ denotes the set of indices of the cells that send synaptic inputs to the i-th cell. We set the bias currents as $I_{{\rm bias},i} = 30, 32, 6, 6.5, 34, 36, 38$ for $i = 1, \ldots, 7$, respectively. For each synaptic current, $I_{{\rm syn},ij}$, we adopted the kinetic synapse model [21] as

$$I_{{\rm syn},ij} = G_{ij}r_{ij}(t)[V_i(t) - E_{ij}].$$

Here, r_{ij} represents the fraction of bound receptor proteins. Its dynamics are given by

$$\frac{dr_{ij}}{dt} = \alpha_{ij}T_{ij}(1-r_{ij}) - \beta_{ij}r_{ij},$$

where T_{ij} denotes the concentration of the neurotransmitter, which is set to 1 when the presynaptic cell emits a spike and then reset to 0 after 1 millisecond. The constants α_{ij} and β_{ij} determine the timescale of the kinetics of r_{ij}, E_{ij} is the reversal potential (in millivolts), and G_{ij} is the synaptic conductance. We used the values $(\alpha_{ij}, \beta_{ij}, E_{ij}, G_{ij}) = (1.1, 0.67, 0, 0.5)$ for excitatory and $(9.8, 0.2, -75, 0.4)$ for inhibitory synapses. For each cell, a weak, independent noise function $\xi_{\cdot,i}$ was added to the membrane voltage V_i and channel variables, m_i, h_i, and n_i. The noise was a Gaussian white noise satisfying $\langle\xi_{x,i}(t)\rangle = 0$ and $\langle\xi_{x,i}(t)\xi_{y,j}(s)\rangle = \sigma_x^2\delta_{xy}\delta_{ij}\delta(t-s)$, where $x, y = V, m, h, n$, and i and j are the cell indices. The noise strengths used are $\sigma_V = 0.5$ and $\sigma_m = \sigma_h = \sigma_n = 5\times10^{-6}$.

V. RESULTS WITH $N = 20$ OSCILLATORY NEURONS.

To examine whether our method yields reasonable estimations for larger networks, we considered a network 20 spiking neurons. The network consists of 16 Hodgkin-Huxley ($i = 1, \ldots, 16$) and 4 fast-spiking ($i = 17, \ldots, 20$) neurons. The induced bias currents were $I_{{\rm bias},i} = 29 + i$ for the Hodgkin-Huxley and $I_{{\rm bias},i} = 6 + 0.25(i-17)$ for the fast-spiking neurons. Unlike in the case of the second example considered in the main text, in the present case, all neurons were active in every trial. All the parameter values were chosen to be the same as in the example with seven neurons, except that the parameter values were chosen as $\sigma_V = 0.1$ and $\sigma_m = \sigma_h = \sigma_n = 1\times10^{-6}$, and $G_{ij} = 0.1$ (0.08) for excitatory (inhibitory) cells. Figure S1 plots the results of the estimation obtained using the voltage trace data, which is five times the size of that in the example with seven neurons. We find that the estimation is sufficiently good that the existence, directionality and heterogeneity of the couplings are all distinguishable, although fine details of the coupling functions are not completely captured.

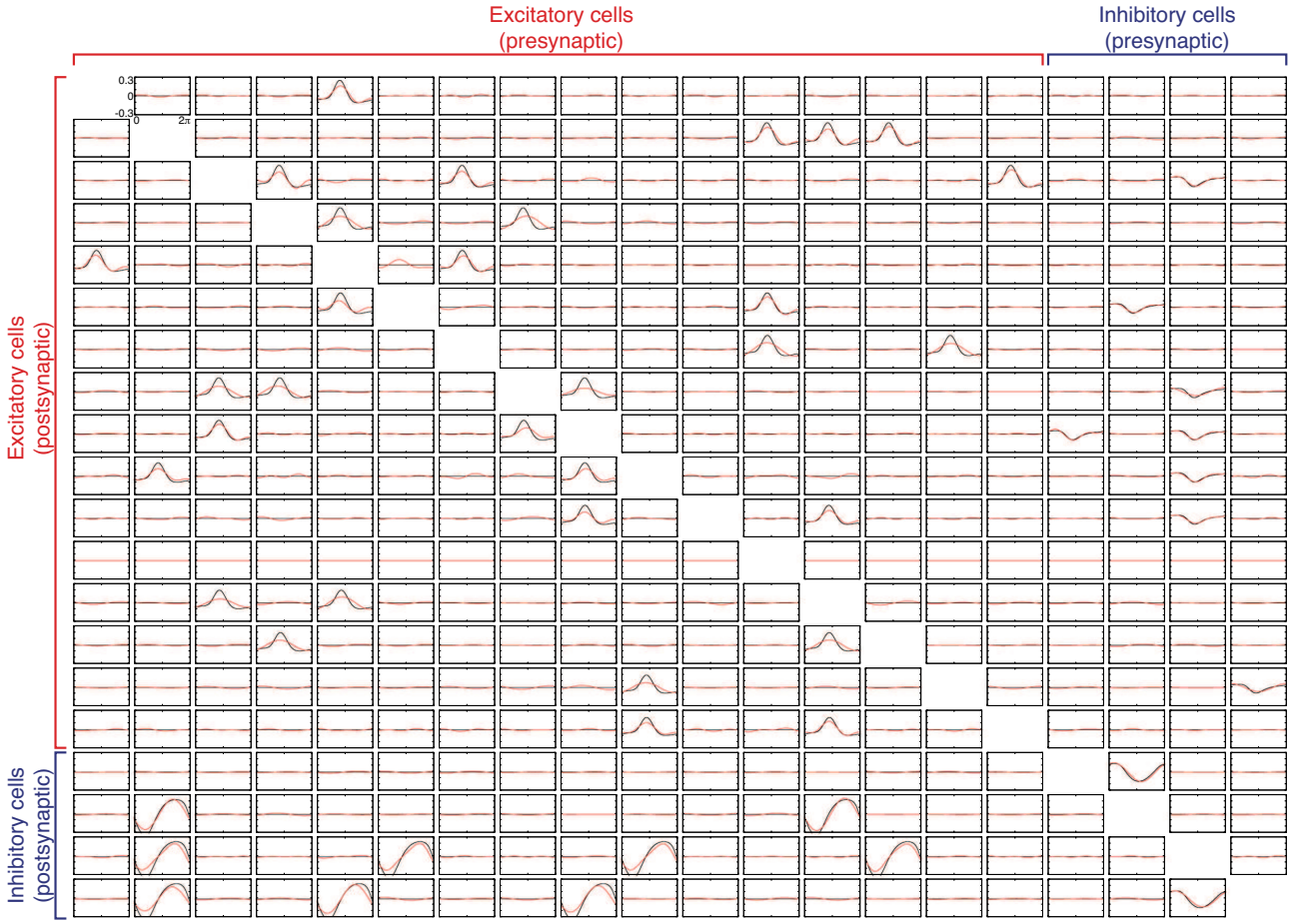

FIG. S1. Estimated (red trace) and true (black trace) coupling functions $\hat{\Gamma}_{ij}$ for the example with twenty neurons. For the estimated curves, the posterior mean is plotted. It should be noted that couplings between distinct types (excitatory and inhibitory) of postsynaptic and presynaptic cells lead to significantly different forms for the coupling functions.

[1] F. C. Hoppensteadt and E. M. Izhikevich, *Weakly Connected Neural Networks* (Springer-Verlag, Berlin, 1997).
[2] U. Alon, *An Introduction to Systems Biology: Design Principles of Biological Circuits* (Chapman and Hall/CRC, Boca Raton, 2006).
[3] M. A. Nowak, *Evolutionary Dynamics: Exploring the Equations of Life* (Belknap Press, Cambridge, 2006).
[4] A. Barrat, M. Barthélemy, and A. Vespignani, *Dynamical Processes on Complex Networks* (Cambridge University Press, Cambridge, 2008).
[5] Y. Kuramoto, *Chemical Oscillations, Waves, and Turbulence* (Springer-Verlag, Berlin, 1984).
[6] S. H. Strogatz, *Sync*, The Emerging Science of Spontaneous Order (Hyperion, New York, 2003).
[7] S. G. Shandilya and M. Timme, New J. Phys. **13**, 013004 (2011).
[8] C. F. Cadieu and K. Koepsell, Neural Comput. **22**, 3107 (2010).
[9] I. T. Tokuda, S. Jain, I. Z. Kiss, and J. L. Hudson, Phys. Rev. Lett. **99**, 064101 (2007).
[10] B. Kralemann, L. Cimponeriu, M. Rosenblum, A. Pikovsky, and R. Mrowka, Phys. Rev. E **76**, 055201 (2007).
[11] B. Kralemann, L. Cimponeriu, M. Rosenblum, A. Pikovsky, and R. Mrowka, Phys. Rev. E **77**, 066205 (2008).
[12] B. Kralemann, A. Pikovsky, and M. Rosenblum, Chaos **21**, 025104 (2011).
[13] T. Stankovski, A. Duggento, P. V. E. McClintock, and A. Stefanovska, Phys. Rev. Lett. **109**, 024101 (2012).
[14] A. Duggento, T. Stankovski, P. V. E. McClintock, and A. Stefanovska, Phys. Rev. E **86**, 061126 (2012).
[15] A. Pikovsky, M. Rosenblum, and J. Kurths, *Synchronization. A Universal Concept in Nonlinear Sciences* (Cambridge University Press, Cambridge, 2004).
[16] See Supplemental Material for details concerning the method and additional results.
[17] C. M. Bishop, *Pattern Recognition And Machine Learning* (Springer, New York, 2006).
[18] K. P. Murphy, *Machine Learning: A Probabilistic Perspective* (The MIT Press, Cambridge, 2012).

[19] A. L. Hodgkin and A. F. Huxley, J. Physiol. **117**, 500 (1952).
[20] A. A. Erisir, D. D. Lau, B. B. Rudy, and C. S. Leonard, J. Neurophysiol. **82**, 2476 (1999).
[21] A. Destexhe, Z. F. Mainen, and T. J. Sejnowski, Neural Comput. **6**, 14 (1994).